IUTAM_ABCM Symposium on Laminar Turbulent Transition

Linear instability analysis of incompressible flow over a cuboid cavity

Q. Liu[a,*], F. Gómez[b], V. Theofilis[a]

[a]*School of Aeronautics, Universidad Politécnica de Madrid, Pza. Cardenal Cisneros 3, E-28040 Madrid, Spain*
[b]*Department of Mechanical and Aerospace Engineering, Monash University, Victoria 3800, Australia*

Abstract

Direct numerical simulations are performed to analyze the three-dimensional instability of flows over three-dimensional cavities. The flow structures at different Reynolds numbers are investigated by using the spectral-element solver nek5000. As the Reynolds number increasing, the lateral wall effects become more important, the recirculation zone shrinks, the front vortex increases and the flow structure inside of the cavity becomes more complex. Results show that the flow bifurcates from a steady state to an oscillatory regime beyond a value of Reynolds number $Re = 1100$.

Selection and peer-review under responsibility of ABCM (Brazilian Society of Mechanical Sciences and Engineering).

Keywords: instability, cavity flow, sensitive structure

1. Introduction

Viscous flows inside three-dimensional open cavities are of significant interest in fluid mechanics research, as it has been comprehensively employed as engineering models for the understanding of different aeronautical devices, such as slotted flats or landing-gear bays. Although their geometrical simplicity, cavity flows are complex; they consists of rich flow phenomena involving shear layer, shock waves, expansion waves and acoustic waves. Nevertheless, this flow has been extensively studied, both experimentally and numerically, for the last six decades cavity[1 2 3 4] and its flow instability characteristics are not yet fully understood, even for the trivial case of an incompressible three-dimensional lid-driven cavity.[2 3]

Concerning the two-dimensional open cavity flow, it is well know the existence of two different instabilities: the shear layer mode (Rossiter mode) and wake modes. Rossiter[5] developed a semi-empirical formula to obtain resonance frequencies by performing extensive experiments of two dimensional compressible cavity flows with different aspect ratio and different Mach number. He described the flow acoustic resonance phenomenon related to the shear layer mode in terms of a feedback process, in which the vortices generated by the shear at the leading lip of cavity impinge on the trailing edge. This process leads to unsteadiness in the flow, which it transmitted to the the leading edge of the cavity, establishing the feedback process. The phenomena is consistent with a Kelvin-Helmholtz instability. Sarohia[3]

experimentally found that this phenomena only occurs when $\sqrt{Re_\theta}L/\theta_0 >\sim 800$, where Re_θ, L, θ_0 and D represent the Reynolds number depending on the boundary layer thickness momentum, cavity length, upstream lip boundary layer thickness momentum and cavity depth respectively.

Gharib & Roshko[7] were the first ones to observe another instability known as wake mode. They performed experiments of incompressible flow over an axisymmetric cavity, and found that as the Reynolds numbers and length or depth of the cavity increased, the flow features were changed substantially. Intuitively, they noticed that the mean streamlines were no longer perpendicular to the lip of cavity and there were no stationary vortex within the cavity, which is different to the shear layer mode. Pereira & Sousa[8] and Colonius et al.[9] also observed the similar flow transitions by performing two-dimensional DNS. Later, Rowley et al.[6] further investigated these self-sustained oscillations, clearly demonstrating that the wake mode occurs in two dimensional compressible flow with longer cavities.

Concerning three-dimensional instability of two-dimensional cavities flows with spanwise direction homogeneously, Rowley et al.[12] and Theofilis & Colonius[13] both used the residual algorithm to recovery the least damped BiGlobal eigenmodes of these flows. In this context, Theofilis[14] also numerically studied the viscous linear stability of incompressible flows inside wall-bounded different cavities. Brés & Colonius[11] reported the instabilities for flow over cavities with length-to-depth aspect ratio of 1, 2 and 4 at low Reynolds number($35 \leq Re_\theta \leq 400$) by means of DNS. Their linear instability results indicate that the three-dimensional instability is related to centrifugal effects. These three-dimensional instabilities have a spanwise wavelength of approximately one cavity depth and oscillate with a frequency about one order of magnitude lower than two-dimensional Rossiter mode. De Vicente et al.[15] established a connection between the onset of the centrifugal instabilities and and the saturated flow by performing numerical and experimental analysis.

To date, the instability analysis of a *fully* three-dimensional cavity flow has not been carried out because of its complex physical characteristics and high computational cost. In this context, only a small number of three-dimensional DNS have been carried out. Larchevêque et al.[25] used large-eddy simulations to investigate the 3D cavity flow with aspect ratio L:D:W=5:1:1 at $Re = 7 \times 10^6$. Yao et al.[26] investigated the unsteady incompressible flow past 3D rectangular cavities at Reynolds number 3, 000 and 10, 000 showing that as the Reynolds number increases the flow goes into the transitional and turbulent regimes. Sarah et al.[27] documented the three-dimensional structure of incompressible flow in the open cavity with aspect ratio length to width-to-depth L:D:W=6:2:1 at low speed with Reynolds $Re = 3.4 \times 10^5$ to $Re = 4.3 \times 10^4$, showing a large recirculate zone, two vortices at the back of cavity and one weak vortex at the front of the cavity.

However, the description of how this flow structures are generated as the Reynolds number increases is still elusive and there are still open question on how the lateral walls affect the instability characteristic of the flow. The present work attempts to provide a preliminary answer to this questions by performing direct numerical simulation of the flow over a rectangular cuboid at low Reynolds number.

2. Problem formulation

2.1. Simulation configuration and fluid properties

The cavity configuration and fluid properties are sketched in Fig1, in which the cavity length L, depth D and width W are defined. Reynolds number $Re = \frac{DU_\infty}{\nu}$ depend on the depth of cavity and the free-stream velocity U_∞. Note that the incoming flow is laminar and a Blasius profile is defined at the inlet boundary condition, in which subscripts 1 and 2 represents the position at inlet and at the lip of the cavity, respectively. A second Reynolds number Re_{δ^*} is defined employing the displacement thickness δ^*. In order to keep the flow laminar when it reaches the cavity, the upstream length is limited by Re_{δ^*}, which needs to be smaller than the critical Reynolds number $Re_{\delta^*} = 520$,[29]. In addition, the boundary layer will establish again downstream of the cavity, so in order to avoid Tollmien-Schlichting waves, the previous criteria must be satisfied again. The numerical values employed for all these parameters as listed in Table 2.

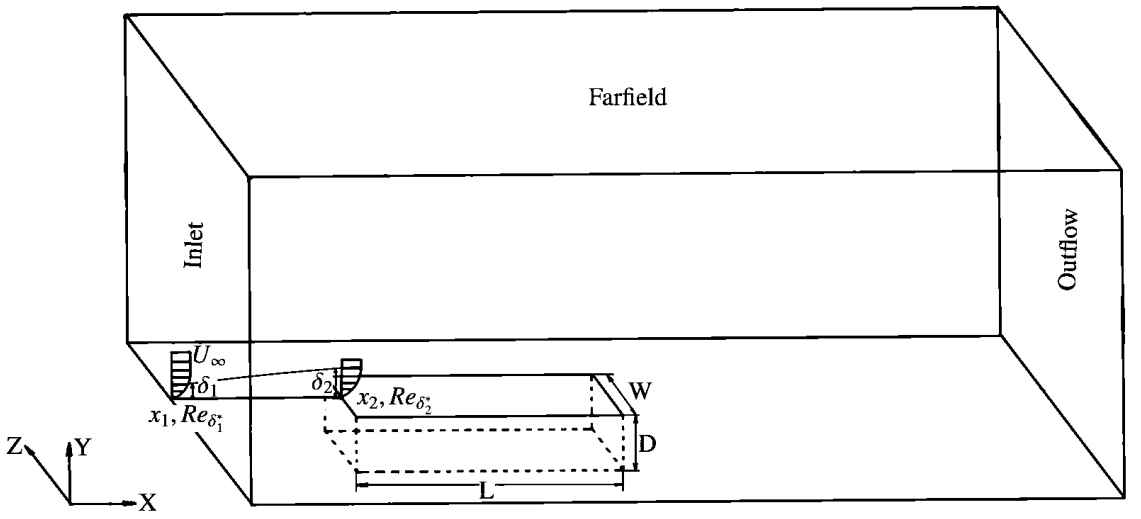

Fig. 1. Computational configuration of full 3D open cavity.

Table 1. Parameters employed for the 3D Open Cavity simulations

Re_D	L/D	Λ/D	θ_2	δ_2^*	$Re_{\delta_2^*}$
500	6	2	0.0515	0.13342	66.708
800	6	2	0.0407	0.10548	84.380
1000	6	2	0.0364	0.0943	94.340
2000	6	2	0.0257	0.0667	133.42

2.2. *Stability analysis*

The flow is governed by the incompressible viscous three-dimensional N-S equations, which read

$$\nabla \cdot U = 0 \tag{1a}$$

$$\frac{\partial U}{\partial t} + U \cdot \nabla U + \nabla P - \frac{1}{Re} \nabla^2 U = 0\,, \tag{1b}$$

where $U = (u, v, w)$ is the velocity vector expressed in Cartesian coordinates (x, y, z) and P is the pressure. No-slip boundary conditions are applied at the wall, the Blasius boundary velocity profile is imposed in the inlet, and the outflow and far-field boundary conditions are Neumann.

The above equation can be decomposed into a steady base flow which is $O(1)$ plus a perturbation $O(\epsilon)$:

$$U(x, y, z, t) = \bar{u}(x, y, z) + \varepsilon \tilde{u}(x, y, z, t) \tag{2a}$$

$$P(x, y, z, t) = \bar{p}(x, y, z) + \varepsilon \tilde{p}(x, y, z, t) \tag{2b}$$

where $\varepsilon << 1$. Substituting Eq. (2) into Eq. (1), reformulating in the perturbation terms, keep the items with same order of magnitude of $O(\varepsilon)$. So we get the linearized Navier-Stokes equations Eq.(3) for describing the evolution of unsteady perturbation.

$$\frac{\partial \tilde{u}}{\partial t} + (\tilde{u} \cdot \nabla)\, \bar{u} + (\bar{u} \cdot \nabla)\, \tilde{u} - \frac{1}{Re} \nabla^2 \tilde{u} + \nabla \tilde{p} = 0 \tag{3a}$$

$$\nabla \cdot \tilde{u} = 0 \tag{3b}$$

Assuming the perturbation is sinusoidal and non-periodic in three spatial directions, corresponding to a TriGlobal linear stability analysis, the perturbation can be simplified as $\tilde{q}(x, y, z, t) = \hat{q}(x, y, z) e^{-i\Omega t} + c.c.$, where $q = (U, P)$, both

Ω and $\hat{q}$ can be complex while $\tilde{q}$ is always real. $\Omega = \omega + i\sigma$, ω is the frequency of the perturbation and σ means damping/growth rate. If the $\sigma > 0$, the perturbation will grow exponential in time and if $\sigma < 0$ the flow is stable.

3. Numerical methods

3.1. Direct numerical simulation

We used nek5000[32] to simulate the 3D cavity flow. This computational fluid dynamics solver is based on a spectral-element method and employs a standard MPI for concurrent execution. The full incompressible N-S equations are solved on a structure mesh, with clustering of points near the wall and the shear layer of the cavity. The computational domain is sub-divided into a number of elements, where the governing equation discretize and cast into variation formulations. The solution is approximated by the Galerkin method as an expansion in a finite set of Legendre basis functions, which together with the corresponding Gauss-Lobatto grid enable exact Gaussian quadrature for the evaluation of the element-wise integrals. Time integration is used Crank-Nicolson for the diffusion term and third-order Adams-Bashforth for the convection term. For the results presented here we used a grid with 30×8×22 elements in the domain above the cavity and $16 \times 6 \times 10$ elements inside the cavity, 6th polynomial order and the computation grid as shown in the Fig.2.

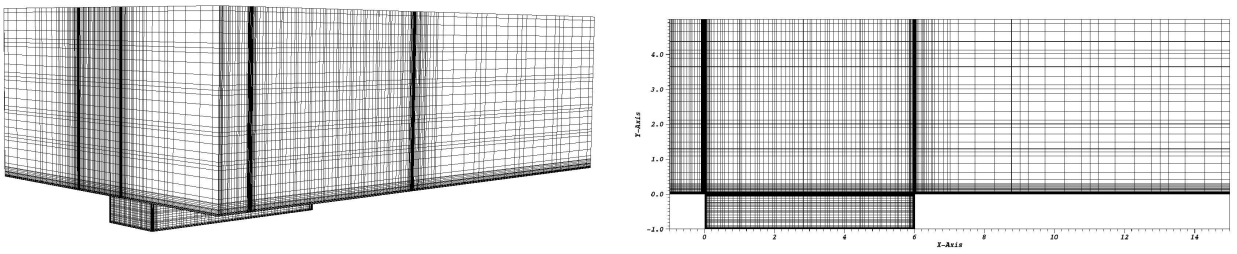

(a) whole grid of the configuration

(b) Slice of grid in the centreline of the cavity

Fig. 2. The computation grid are employed in the direct numerical simulations.

3.2. Residual algorithm and global modes

The Residual Algorithm (RA) is the method to extract the global modes resulting from a transient simulation data or experiment. When the time-accurate integration of the equations of motion approaches a steady state, it is possible to extract information about the damping rate and amplitude functions of decaying linear global modes. Further details of this algorithm can be found in the previous research [13,39,40,21] .

In particular, if the time-accurate integration is close to convergence, considering the transient solution from two time levels, t_1 and t_2, the steady-state flow and the eigenmodes can be obtained from a system of algebraic equations. Then, by performing simple algebraic operations, we can recover the base flow $\bar{q}(x, y, z)$ and the eigenmodes $\hat{q}(x, y, z)$.

Consider that $\tilde{q}(x, y, z, t) = \hat{q}e^{-i\Omega t}$, within a numerical point of view, represents the rate at which the residuals $\tilde{q}(x, y, z, t)$ decay in the neighborhood of $\bar{q}$. Note that we treat Ω as a pure imaginary number ($\Omega = i\sigma, \omega = 0$) for simplicity the problem. We then recover the parameter Ω by monitoring the solution at two time levels, t_1 and t_2 as

$$q(x, y, z, t_1) = \bar{q}(x, y, z) + \varepsilon\hat{q}e^{\sigma t_1} \tag{4a}$$

$$q(x, y, z, t_2) = \bar{q}(x, y, z) + \varepsilon\hat{q}e^{\sigma t_2}\,. \tag{4b}$$

Combining these two equations, it follows that the time-behavior of the solution may be monitored by

$$\sigma = \frac{ln(\epsilon(t_1)/\epsilon(t_2))}{t_1 - t_2} \tag{5}$$

where $\epsilon(t) = |q(x, y, z, t) - \bar{q}(x, y, z)|$.

4. Results

4.1. Validation: lid-driven cavity

First, the base flow of a 3D lid-driven cavity at Re=1000 have served as validation case of the Nek5000 in DNS mode. The obtained steady-state solution has been compared with the literature[28,23], as shown in Table 2. As the resolution increase, the velocity in the middle of the lid-driven cavity does not change, which proves grid independence.

Table 2. Comparison with the spectral-element method (SEM) nek5000 own results, benchmark spectral collocation method[28] (SCM) and results Finite volume method[23] (FVM) of the minimum and maximum velocities on the centerlines for the 3D lid-driven cavity at Re=1000.

Method	AR	N_x	N_y	N_z	v_{min}	x	v_{max}	x	u_{min}	y
SCM	1 : 1 : 1	96	96	96	−0.4350	0.9096	0.2466	0.1091	−0.2803	0.1242
FVM	1 : 1 : 1	144	144	144	−0.4333	0.9076	0.2456	0.1073	−0.2792	0.1235
SEM	1 : 1 : 1	96	96	96	−0.4350	0.9096	0.2466	0.1090	−0.2803	0.1244
SEM	1 : 1 : 1	64	64	64	−0.4348	0.9104	0.2466	0.1104	−0.2800	0.1296

4.2. 3D open cavity flow

Table 3 shows the damping ratio of the least-stable eigenmodes of the flow over the rectangular cuboid cavity at Reynolds numbers from 500, 800,1000,1100 and 2000. Correspondingly, Fig.4, 5, 6, 7 show the eigenfunctions associated to these eigenvalues. Additionally, Fig 3 shows how the spanwise velocity w of the base flow changes with the Reynolds number. We observe that the steady instability modes become traveling as the Reynolds number increases and that at Re=1100 the damping rate become small $\sigma \sim O(-1 \times 10^{-5})$, indicating neutral stability and the onset of a Hopf bifurcation with frequency is $\omega = 0.229$. This is confirmed with results at Reynolds $Re = 2000$, indicating that the flow become unsteady and non-linear, as shown in the Fig.3(f).

5. Summary

Instability of incompressible flow over a cuboid cavity with aspect ratio L:D:W=6:2:1 has been investigated using the spectral-element solver nek5000[32]. Results indicate the critical Reynolds number at these conditions is $1100 \leq Re_{\text{cr}} \leq 1200$. The least damped three-dimensional eigenmodes were computed using the Residual Algorithm[13,40]. Their structure reveals that instability is confined in the neighborhood of the cavity region, and that the lateral walls strongly modify the structure of linear perturbations of the cuboid, compared with those of the equivalent spanwise homogeneous cavity flow[11].

Work is in progress, examining the critical conditions at different three-dimensional aspect ratio values, as well as performing accompanying DNS work in order to follow linear instability into transition. Results will be reported elsewhere.

Table 3. Effect of the Reynolds number on the least eigenvalues of the flow over a cuboid cavity extracted by residual algorithm to DNS.

Re	Ω_1	Ω_2
500	$-i \cdot 0.098$	
800	$-i \cdot 0.054$	
1000	$0.0123 - i \cdot 0.0115$	$0.229 - i \cdot 0.175$
1100	$\sim 0.229 - i \cdot O(-1 \times 10^{-5})$	

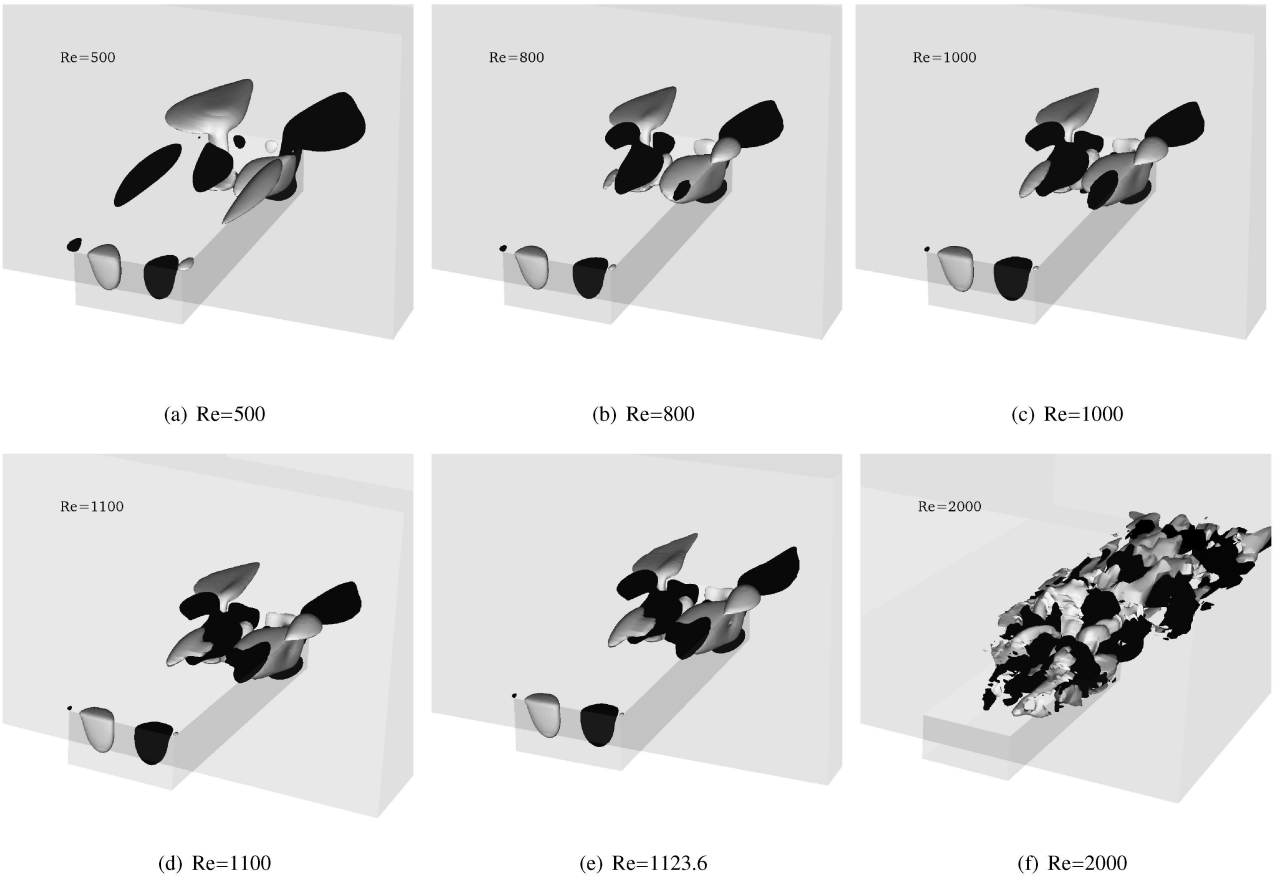

(a) Re=500 (b) Re=800 (c) Re=1000

(d) Re=1100 (e) Re=1123.6 (f) Re=2000

Fig. 3. Instantaneous spanwise velocity components in the 3D open cavity cases with different Reynolds numbers. The iso-surfaces represent the spanwise velocity levels $w/U = -0.008$ and $w/U = 0.008$, except for Re=2000, the velocity levels is $w/U = -0.05$ and $w/U = 0.05$.

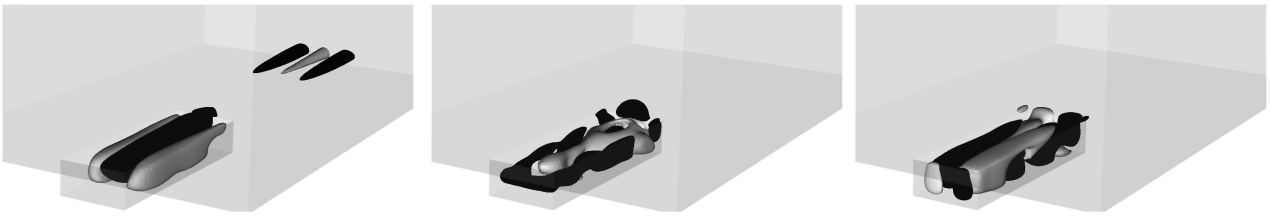

(a) $\hat{u}$ (b) $\hat{v}$ (c) $\hat{w}$

Fig. 4. Real part of the eigenfunction velocity field ($\hat{u}$,$\hat{v}$,$\hat{w}$=±0.1) of the full 3D open cavity at Re=500 which corresponding to the least stationary mode $\Omega = i \cdot (-0.0983)$

(a) $\hat{u}$ (b) $\hat{v}$ (c) $\hat{w}$

Fig. 5. Real part of the eigenfunction velocity field ($\hat{u}$,$\hat{v}$,$\hat{w}$=±0.1) of the full 3D open cavity at Re=800 which corresponding to the least stationary mode $\Omega = i \cdot (-0.0538)$

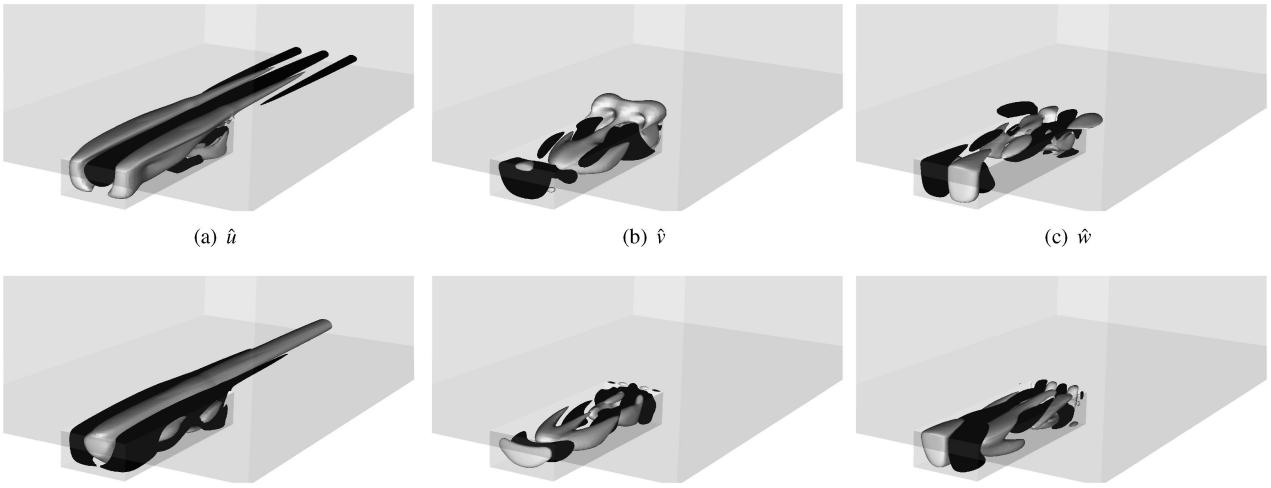

(a) $\hat{u}$ (b) $\hat{v}$ (c) $\hat{w}$

(d) $\hat{u}$ (e) $\hat{v}$ (f) $\hat{w}$

Fig. 6. Real part of the eigenfunction velocity field ($\hat{u}$,$\hat{v}$,$\hat{w}$=±0.1) of the full 3D open cavity at Re=1000, there two modes, mode I (a-c) $\Omega = 0.2295 + i \cdot (-0.1749)$ and mode II (d-f) $\Omega = 0.0123 + i \cdot (-0.0115)$.

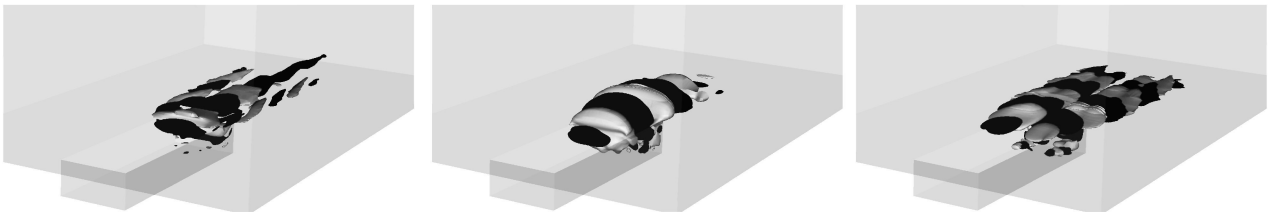

(a) $\hat{u}$ (b) $\hat{v}$ (c) $\hat{w}$

Fig. 7. Real part of the eigenfunction velocity field ($\hat{u}$,$\hat{v}$,$\hat{w}$=±0.1) of the full 3D open cavity at Re=1100 which corresponding to the least traveling mode $\Omega = 0.2289 + i \cdot (-0.000014)$

References

1. Roshko, A. Some measurements of flow in a rectangular cutout.*NACA TN* 1955;3488.
2. K. Krishnamurty, Acoustic radiation from two dimensional rectangular cutouts in aerodynamic surfaces. *NACA TN* 1955; 3487.
3. Sarohia, V. Experimental and analytic investigation of oscillations in flows over cavities.*PhD thesis, California Institute of Technology.* 1975
4. Sarohia, V. Experimental investigation of oscillations on flows over shallow cavities.*AIAA Journal* 1977;**15**: 984-991.
5. J. Rossiter. Wind-tunnel experiments on the flow over rectangular cavities at subsonic and transonic speeds. *Aeronautical research council reports and memoranda.* 1964; 3438
6. C. W. Rowley, T. Colonuis, A. J. Basu. On self-sustained oscillations in two-dimensional compressible flow over rectangular cavities. *J. Fluid Mech.* 2002; **455**:315-346
7. M. Gharib, A. Roshko. The effect of flow oscillations on cavity drag. *J. Fluid Mech.* 1987; **177**:501-530
8. Pereira, J.C.F., J.J.M.Sousa. Influence of impingement edge geometry on cavity flow oscillations. *AIAA Journal.* 1994; **32**: 1737-1740.
9. Colonius, T., Basu, A. J., Rowley, C. W. Numerical investigation of the flow past a cavity. *AIAA Paper*,1999: 99-1912.
10. G. A. Brés. Numerical simulations of three-dimensional instabilities in cavity ows. *PhD thesis*, California Institute of Technology. 2007.
11. G. A. Brés, T. Colonius. Three dimensional instabilities in compressible flow over open cavity. *J. Fluid Mech.* 2008; **599** :309-339
12. C. W. Rowley, V. Theofilis, T. Colonius. Numerical simulation of three-dimensional instabilities in cavity flow. *J. DLR-Mitteilung* 2001.
13. V. Theofilis, T. Colonius. An algorithm for the recovery of 2-D and 3-D biglobal instabilities of compressible flow over 2-D open cavities. *AIAA paper*, 2003; 2003-4143
14. V. Theofilis, P.W. Duck, J. Owen. Viscous linear stability analysis of rectangular duct and cavity flows. *J. Fluid Mech.* 2004; **505** :249-286
15. De Vicente, J., Basley, J., Meseguer-Garrido, F., Soria, J., V. Theofilis. Three dimensional instabilities over a rectangular open cavity: from linear stability analysis to experimentation. *J. Fluid Mech.* 2014;**748**, 189-220.
16. De Vicente, J. Spectral multidomain method for the global instability analysis of complex cavity flow. *PhD thesis*, Universidad Politécnica de Madrid. 2010.
17. Maull, D. J., East, L. F. Three dimensional flow in cavities. *J. Fluid Mech.*, 1963, **16**: 620-632.
18. Pan, F., Acrivos, A. Steady flow in rectangular cavity. *J. Fluid Mech.*, 1976, **28**: 643-655.
19. Koseff, J. R., Street, R. L. On end wall effects in a lid-driven cavity. *J. Fluids Eng.*, 1984 *106*: 385-389.
20. Aidun, C. K., Triantafillopoulos, N. G., Benson, J. D. Global stability of a lid-driven cavity with through flow: flow visualization studies. *Phys. Fluids*, 1991 **A3**: 2081-2091.
21. F. Gómez., Clainche, S. Le, Paredes, P., Hermanns, M., Theofilis, V. Four decades of studying global linear instability: Progress and challenges. *AIAA Journal*, 2012 **50**: 2731-2743.
22. F. Gómez., Theofilis, V., Paredes, P., Liu, Q., He, W., On the role of global flow instability analysis in closed loop flow control. *AIAA Paper*, 2012-2679
23. F. Gómez., R. Gómez, Theofilis, V., On the three-dimensional global linear instability analysis of flow with standard aerodynamics codes. *Aerospace Sciences and Technology*, 2014, **32**: 223-234.
24. F. Gómez. *PhD thesis*, Matrix-free time-stepping methods for solution of TriGlobal instability problems, Universidad Politécnica de Madrid. 2010.
25. Larchevêque, L., Sagaut, P., Lê, T. H., Comte, P., Large-eddy simulation of compressible flow in a three-dimensional open cavity at high Reynolds number. *J. Fluid Mech.*, 2004, **516**: 265-301.
26. Yao, H., Cooper, R. K., Raghunathan, S. Numerical simulation of incompressible laminar flow over three dimensional rectangular cavities. *Journal of Fluid Engineering*, 2004, **126**: 919-927.
27. Sarah D. Crook, Timothy C. Wu. Lau, Richard M. Kelso, Three-dimensional flow within shallow narrow cavities, *J. Fluid Mech.*, 2013, **725**: 587-612.
28. Albensoeder, S., Kuhlmann, H. Accurate three-dimensional lid-driven cavity flow. *Journal of Computational Physics*, 2005,**206**: 536-558.
29. G. B. Schubauer, H. K. Skramstad, Laminar boundary layer oscillation and transition on a flat plate, *NACA Rep.* 1943, 909.
30. F. Giannetti, P. Luchini, Structure sensitivity of the first instability of the cylinder wake, *J. Fluid Mech.*, 2007, **581**: 167
31. J.M. Chomaz, Global Instabilities in Spatially Developing Flows: Non-Normality and Nonlinearity. *Annu. Rev. Fluid Mech.*, 2005, **37**: 357392.
32. Paul F. Fischer, Gerald W. Kruse, Francis Loth. Spectral element methods for transitional flows in complex geometries. *Journal of Scientific Computing*,2002,**17**: 87-106.
33. R. Issa, Solution of implicitly discretized fluid flow equations by operator-splitting, *Journal of Computational Physics*, 1986, **62**: 40-65.
34. H. Jasak, Error analysis and estimation for the finite volume method and applications to fluid flows. *Ph.D. thesis*, Imperial College, 1996.
35. J. Ferziger, M. Peric. Computational methods for fluid dynamics, Springer, 2001.
36. E. Sanmiguel-Rojas, J. Jimenez-Gonzales, P. Bohorquez, G. Pawlak. C. Martínez-Bazán, Effect of base cavities on the stability of the wake behind slender blunt-based axisymmetric bodies, *Physics of Fluids* , 2011, **23**.
37. P. Bohorquez, E. Sanmiguel-Rojas, A. Sevilla, J. Jimenez-Gonzales, C. Martínez-Bazán, Stability and dynamics f the laminar wake past a slender blunt-based axisymmetric body, *J. Fluid Mech.* 2011, **676**: 110-144.
38. P. Bohorquez, L. Parras, Three-dimensional numerical simulation of the wake flow of an afterbody at subsonic speeds. *Theor. Comp. Fluid Dyn.* 2012.
39. V. Theofilis, Global linear instability. *Annual Review of Fluid Mechanics*, 2011, **43**: 319-352.
40. V. Theofilis, On steady-state flow solutions and their nonparallel global linear instability. *Advances in Turbulence*, 2000, **8**: 35-38.